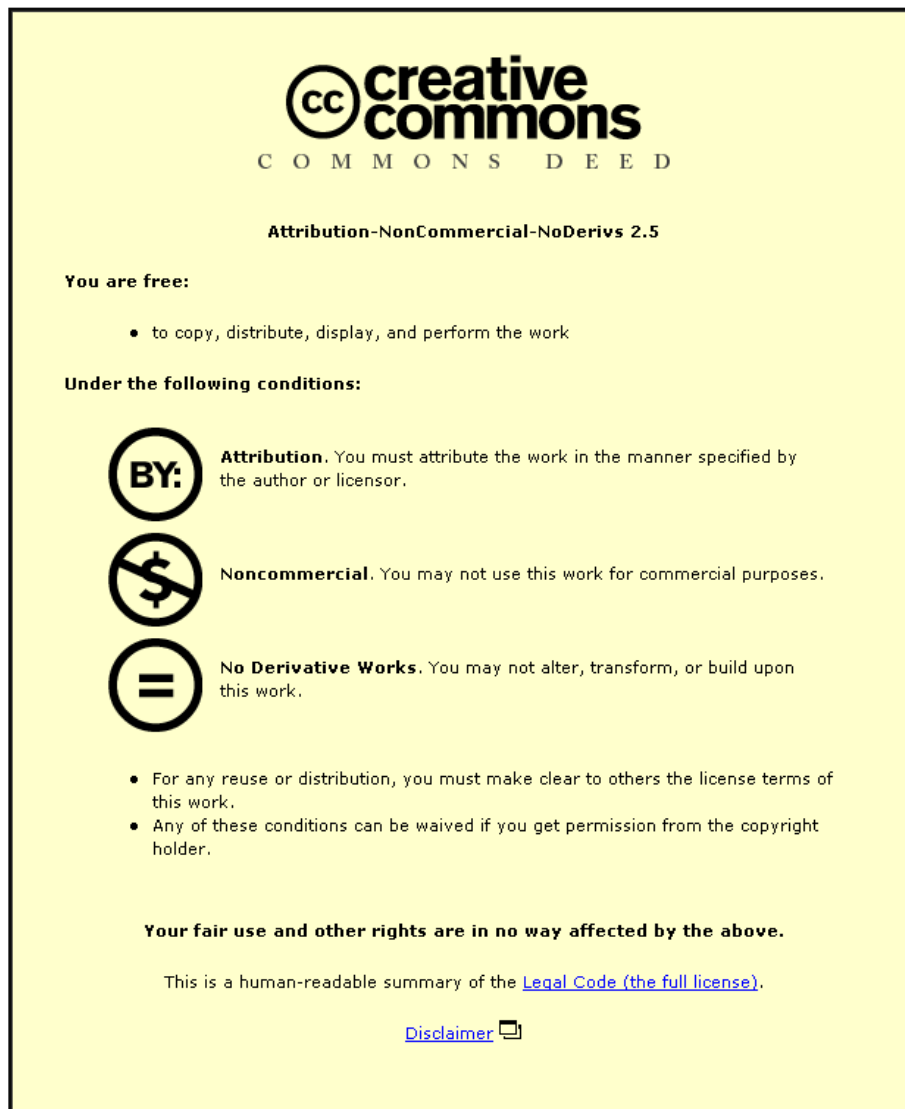


This item was submitted to Loughborough's Institutional Repository (<https://dspace.lboro.ac.uk/>) by the author and is made available under the following Creative Commons Licence conditions.



For the full text of this licence, please go to:
<http://creativecommons.org/licenses/by-nc-nd/2.5/>

Prediction of oil-film thickness and shape in elliptical point contacts under combined rolling and sliding motion

D Jalali-Vahid¹, H Rahnejat^{1*}, R Gohar² and Z M Jin¹

¹Department of Mechanical Engineering, University of Bradford, UK

²Department of Mechanical Engineering, Imperial College of Science, Technology and Medicine, London, UK

Abstract: The paper presents a numerical solution for elliptical point contact conjunctions under combined rolling and sliding motion. This condition is prevalent in many practical applications, such as rolling element bearings and conformal gears. An effective influence Newton–Raphson method is employed in local point distributed or global line distributed low-relaxation iterations. This method enables determination of the pressure distribution and film shape at high loads such as are encountered in many practical applications. Some of the numerical predictions have been validated against experimental results.

Keywords: oil-film thickness, oil-film shape, elliptical point contacts, combined rolling and sliding motion

NOTATION

a	semimajor axis of contact ellipse in the transverse direction y	H	dimensionless film thickness = hR_x/b^2
b	semiminor axis of contact ellipse in the entraining direction x	H_0	dimensionless constant defined in equation (7)
D	deformation matrix	K	ellipticity parameter = a/b
E	modulus of elasticity	\bar{l}	constant used to determine the length of the side leakage region
E'	equivalent Young's modulus = $2/[(1 - \nu_A^2)/E_A + (1 - \nu_B^2)/E_B]$	\hat{l}	dimensionless constant used to determine the length of the side leakage region
G^*	material parameter = $\alpha E'$	\bar{m}	constant used to determine the length of the inlet region
h	film thickness	\hat{m}	dimensionless constant used to determine the length of the inlet region
h_{\min}	minimum film thickness	n_x	number of nodes in the x direction
\bar{h}_{cen}	central film thickness obtained from the current numerical solution	n_y	number of nodes in the y direction
\bar{h}_{\min}	minimum film thickness obtained from the current numerical solution	p	pressure
\tilde{h}_{cen}	central film thickness obtained by Chittenden <i>et al.</i> [3, 4]	P	dimensionless pressure = p/P_H
\tilde{h}_{\min}	minimum film thickness obtained by Chittenden <i>et al.</i> [3, 4]	P_H	Hertzian pressure
\hat{h}_{cen}	central film thickness obtained by Mostofi and Gohar [2]	$P_{H \max}$	maximum Hertzian pressure
\hat{h}_{\min}	minimum film thickness obtained by Mostofi and Gohar [2]	R_e	equivalent radius of contact in the entraining direction, $1/R_e = (\cos^2 \theta)/R_x + (\sin^2 \theta)/R_y$
		R_x	equivalent radius of contact in the x direction
		R_y	equivalent radius of contact in the y direction
		t	time
		u_{av}	mean velocity components in the x direction = $(u_A + u_B)/2$
		u_A	surface velocity of solid A in the x direction
		u_B	surface velocity of solid B in the x direction
		U_e	equivalent velocity in the entraining direction = $(u_{av}^2 + v_{av}^2)^{1/2}$
		U^*	dimensionless velocity = $u\eta_0/(E'R_x)$

The MS was received on 2 March 2000 and was accepted after revision for publication on 4 April 2000.

*Corresponding author: Department of Mechanical Engineering, University of Bradford, Bradford BD7 1DP, UK.

u_{av}	mean velocity component in the y direction $= (v_A + v_B)/2$
v_A	surface velocity of solid A in the y direction
v_B	surface velocity of solid B in the y direction
W	normal applied load
W_e	dimensionless load $= W/(E' R_e^2)$
W^*	dimensionless load $= W/(E' R_x^2)$
x	Cartesian coordinate
X	$= x/b$
ΔX	distance between two neighbouring points in the X direction
y	Cartesian coordinate
Y	$= y/a$
ΔY	distance between two neighbouring points in the Y direction
z	viscosity–pressure index
α	pressure–viscosity coefficient ($m^2 N$)
δ	total elastic deformation
θ	entraining angle with the x direction $= \tan^{-1}(u_{av}/v_{av})$
η	lubricant viscosity
η_0	atmospheric viscosity
$\bar{\eta}$	dimensionless lubricant viscosity $= \eta/\eta_0$
ν	Poisson's ratio
ρ	lubricant density
ρ_0	atmospheric density
$\bar{\rho}$	dimensionless density $= \rho/\rho_0$
Ω	under-relaxation factor

1 INTRODUCTION

Most elasto-hydrodynamic studies which have been concerned with the determination of oil-film shape and thickness, either through optical interferometry or by numerical prediction, deal with circular point contacts or elliptical point contacts with oil flow taking place along one of the principal axes of the Hertzian elastostatic ellipse. Under practical conditions in the rolling and sliding contact of balls in raceway grooves the direction of lubricant entrainment may be inclined to the rolling axis. These conditions are sometimes further complicated by ball spin due to a gyroscopic moment. The direction of entraining motion and indeed the inclination of the elliptical contact also alter in meshing conformal gear teeth, although in some cases such as Novikov gears the large contact dimensions may make the use of Hertzian theory rather suspect. Optical interferometric studies for elliptical point contact conditions, varying the direction of lubricant entrainment, have been reported by Thorp and Gohar [1]. In their work a ball sliding in a stationary conforming groove was investigated under low generated pressures, with the contiguous surfaces having low distortions. Although such

conditions are useful to investigate, they are seldom found to be practical.

Numerical predictions for oil-film thickness and shape have been reported by Mostofi and Gohar [2] and Chittenden *et al.* [3, 4]. The former have shown good agreement between their numerical results and the experimental work in reference [1]. The latter have shown that the central oil-film thickness is little affected by the orientation of the lubricant entraining vector, but the minimum film thickness values cover a much broader range than those obtained when the direction of entraining motion is along the minor axis of the Hertzian ellipse. They have shown that the minimum film thickness h_{min} occurs in the side lobes in the vicinity of the Hertzian lateral boundaries. However, all the contributions [2–4] are at low loads. The need for more representative experimental and numerical studies in line with practical conditions is thus evident.

This paper outlines solutions for combined rolling and sliding motion in elliptical contacts, with the direction of lubricant entrainment being inclined to the principal axes of the Hertzian elastostatic ellipse. The numerical method uses the low-relaxation effective influence Newton–Raphson (EIN) iterative method for the local point distributed solution of the five Jacobian terms in the tridiagonal matrix formulation of the Reynolds equation, enabling rapid convergence to occur at high loads. In the case of flow along the major axis of the elastostatic Hertzian contact ellipse, the local point distributed solution was found to exhibit convergence difficulties. In this case a line distributed solution for the five Jacobian terms was employed, following the EIN method outlined by Dowson and Wang [5]. The numerical predictions have been compared with the experimental work reported in reference [1] and the numerical results in references [3] and [4] but extended to much higher loads.

2 THEORETICAL FORMULATION

The dimensional Reynolds equation for an elliptical point contact is given as

$$\begin{aligned} & \frac{\partial}{\partial x} \left(\frac{\rho h^3}{12\eta} \frac{\partial p}{\partial x} \right) + \frac{\partial}{\partial y} \left(\frac{\rho h^3}{12\eta} \frac{\partial p}{\partial y} \right) \\ &= \frac{\partial}{\partial x} \left[\frac{\rho h (u_A + u_B)}{2} \right] + \frac{\partial}{\partial y} \left[\frac{\rho h (v_A + v_B)}{2} \right] \\ &+ \frac{\partial(\rho h)}{\partial t} \end{aligned} \quad (1)$$

where the following dimensionless groups apply:

$$X = \frac{x}{b}, \quad x = bX$$

$$Y = \frac{y}{a}, \quad y = aY$$

$$\hat{m} = \frac{\bar{m}}{b}, \quad \bar{m} = \hat{m}b$$

$$\hat{l} = \frac{\bar{l}}{a}, \quad \bar{l} = \hat{l}a$$

$$\bar{\rho} = \frac{\rho}{\rho_0}, \quad \rho = \rho_0 \bar{\rho}$$

$$\bar{\eta} = \frac{\eta}{\eta_0}, \quad \eta = \eta_0 \bar{\eta}$$

$$H = \frac{hR_x}{b^2}, \quad h = \frac{Hb^2}{R_x}$$

$$U^* = \frac{u_{av}\eta_0}{R_x E'}, \quad u_{av} = \frac{U^* R_x E'}{\eta_0}$$

$$P = \frac{p}{P_H}, \quad p = P_H P$$

$$W^* = \frac{W}{E' R_x^2}, \quad W = W^* E' R_x^2$$

$$G^* = \alpha E'$$

(2)

Thus

$$\begin{aligned} & \frac{\partial}{\partial X} \left(\frac{\bar{\rho} H^3}{\bar{\eta}} \frac{\partial P}{\partial X} \right) + \frac{1}{K^2} \frac{\partial}{\partial Y} \left(\frac{\bar{\rho} H^3}{\bar{\eta}} \frac{\partial P}{\partial Y} \right) \\ & = \psi \left[u_{av} \frac{\partial(\bar{\rho} H)}{\partial X} + \frac{1}{K} v_{av} \frac{\partial(\bar{\rho} H)}{\partial Y} \right] \end{aligned} \quad (3)$$

where

$$\psi = \frac{12\eta_0 R_x^2}{P_H b^3} \quad (4)$$

All the variables in the equations presented in this section are defined in the notation.

The lubricant density variation with pressure is defined by Dowson and Higginson [6] as

$$\bar{\rho}(P) = 1 + \frac{\varepsilon P_H P}{1 + \zeta P_H P} \quad (5)$$

where ε and ζ are constants related to the type of lubricant employed.

The lubricant viscosity variation with pressure has been given by Roelands [7] as

$$\bar{\eta} = \left(\frac{\eta_\infty}{\eta_0} \right)^{1 - (1 + P_H P / \gamma)^z} \quad (6)$$

where z is the viscosity pressure index, $\eta_\infty = 0.631 \times 10^{-4}$ Pa s and $\gamma = 1.9609 \times 10^8$ N/m².

The elastic film shape in dimensionless form is

$$\begin{aligned} H(X, Y) = & H_0 + \frac{(X - \hat{m})^2}{2} \\ & + \frac{R_x}{R_y} K^2 \frac{(Y - \hat{l})^2}{2} + \frac{R_x \delta(X, Y)}{b^2} \end{aligned} \quad (7)$$

where the dimensional elastic deformation at any point (X, Y) is defined as

$$\delta_{I,J} = \frac{2}{\pi} \sum_{j=1,2,\dots}^{n_y} \sum_{i=1,2,\dots}^{n_x} P_{i,j} D_{i^*,j^*} \quad (8)$$

where

$$\begin{aligned} i^* &= |I - i| + 1 \\ j^* &= |J - j| + 1 \end{aligned}$$

The integrated elastohydrodynamic pressure distribution over the contact must satisfy the load balance requirement as

$$\int_{-\infty}^{\infty} \int_{-\infty}^{\infty} P \, dX \, dY = \frac{2\pi}{3} \quad (9)$$

A modified Newton–Raphson method is applied for a low-relaxation solution of the Reynolds equation in the following numerical form:

$$\begin{aligned} & \sum_{k=2}^{n_x-1} \sum_{l=2}^{n_y-1} J_{ij,kl} \Delta P_{k,l} = -F_{i,j}, \\ & 2 \leq i \leq n_x - 1, 2 \leq j \leq n_y - 1 \end{aligned} \quad (10)$$

where

$$\begin{aligned}
 F_{i,j} = & \frac{1}{2\Delta X^2} \left[\left(\frac{\bar{\rho}H^3}{\bar{\eta}} \right)_{i+1,j} + \left(\frac{\bar{\rho}H^3}{\bar{\eta}} \right)_{i,j} \right] P_{i+1,j} \\
 & + \frac{1}{2\Delta X^2} \left[\left(\frac{\bar{\rho}H^3}{\bar{\eta}} \right)_{i,j} + \left(\frac{\bar{\rho}H^3}{\bar{\eta}} \right)_{i-1,j} \right] P_{i-1,j} \\
 & + \frac{1}{2\Delta Y K^2} \left[\left(\frac{\bar{\rho}H^3}{\bar{\eta}} \right)_{i,j+1} + \left(\frac{\bar{\rho}H^3}{\bar{\eta}} \right)_{i,j} \right] P_{i,j+1} \\
 & + \frac{1}{2\Delta Y K^2} \left[\left(\frac{\bar{\rho}H^3}{\bar{\eta}} \right)_{i,j} + \left(\frac{\bar{\rho}H^3}{\bar{\eta}} \right)_{i,j-1} \right] P_{i,j-1} \\
 & - \frac{1}{2\Delta X^2} \left[\left(\frac{\bar{\rho}H^3}{\bar{\eta}} \right)_{i+1,j} + 2 \left(\frac{\bar{\rho}H^3}{\bar{\eta}} \right)_{i,j} \right. \\
 & \quad \left. + \left(\frac{\bar{\rho}H^3}{\bar{\eta}} \right)_{i-1,j} \right] P_{i,j} \\
 & - \frac{1}{2\Delta Y K^2} \left[\left(\frac{\bar{\rho}H^3}{\bar{\eta}} \right)_{i,j+1} + 2 \left(\frac{\bar{\rho}H^3}{\bar{\eta}} \right)_{i,j} \right. \\
 & \quad \left. + \left(\frac{\bar{\rho}H^3}{\bar{\eta}} \right)_{i,j-1} \right] P_{i,j} \\
 & - \varphi \left[u_{av} \frac{(\bar{\rho}H)_{i+1,j} - (\bar{\rho}H)_{i,j}}{\Delta X} \right. \\
 & \quad \left. + \frac{1}{K} v_{av} \frac{(\bar{\rho}H)_{i,j+1} - (\bar{\rho}H)_{i,j}}{\Delta Y} \right] \tag{11}
 \end{aligned}$$

and $J_{ij,kl}$ is the Jacobian matrix which is defined as follows:

$$J_{ij,kl} = \frac{\partial F_{i,j}}{\partial P_{k,l}} \tag{12}$$

The expanded Jacobian terms have been provided in reference [8].

The iterative scheme employs line distributed under-relaxation, as indicated by the following relations:

$$\begin{aligned}
 \Delta P_{k,l}^{new} = & \\
 & \frac{-F_{k,l}^J - (J_{kl,k-1l} \Delta P_{k-1,l}^{new}) - (J_{kl,k+1l} \Delta P_{k+1,l}^{old})}{J_{ij,kl}} \\
 & \quad - (J_{kl,kl-1} \Delta P_{k,l-1}^{new}) - (J_{kl,kl+1} \Delta P_{k,l+1}^{old}) \tag{13}
 \end{aligned}$$

$$P_{i,j}^{new} = P_{i,j}^{old} + \Omega \Delta P_{i,j} \tag{14}$$

where Ω is the under-relaxation factor.

The convergence criteria for pressure and contact load are adhered to as follows:

$$\left[\frac{\sum_i \sum_j (P_{i,j}^{new} - P_{i,j}^{old})^2}{n_x n_y} \right]^{1/2} \leq 10^{-4} \tag{15}$$

$$\left| \iint P(X, Y) dX dY - \frac{2}{3}\pi \right| \leq 10^{-4} \tag{16}$$

3 NUMERICAL RESULTS

The solutions obtained by traditional finite difference relaxation using Gauss–Seidel iterations presented by Chittenden *et al.* [3, 4] were at low values of loads, with the equivalent dimensionless load W_e in the range 0.6238×10^{-8} – 2.4950×10^{-8} , where $W_e = W/(R_e^2 E')$, R_e being the effective radius in the entraining direction. The other problem with the solutions in references [3] and [4] is due to the use of a coarse computational grid of only 57×25 points for an ellipticity ratio of 2.5.

The solutions obtained here, while being in concordance with the results of Chittenden *et al.* at the lower values of load, vary in the range $W^* = 9.21 \times 10^{-7}$ – 1.10×10^{-4} ; these values are far in excess of those in reference [4] and can lead to a maximum Hertzian pressure $P_{Hmax} = 4$ GPa at high loads. The computational grid employed was 133×129 .

Figures 1a and b show the three-dimensional pressure distribution and film shape respectively for $W^* = 2.94 \times 10^{-6}$, which corresponds to a normal load of 400 N. This is a reasonable practical load per ball in, for example, a deep groove ball bearing of 40 mm bore, with a ball diameter of 12.7 mm, where the contact load was shown to oscillate between 100 and 400 N [9]. The conditions pertain typically to a ball orbital position in transition from the loaded region of the bearing to the unloaded region, with the entrainment flow taking place at an angle of 67.5° due to a combined rolling and sliding motion. Figure 1c shows the corresponding oil-film contour, indicating the inclined flow direction. The minimum oil-film thickness regions occur in the side lobes in the contact as also predicted by Chittenden *et al.* [3, 4] under similar conditions. However, due to the skewed flow condition the minimum exit film appears in an asymmetrical position.

Verification of numerical predictions have been carried out against the experimental photomicrographs, reported in reference [1]. Figures 2a and b illustrate oil-film contours obtained numerically under the same conditions as those found experimentally by Thorp and Gohar [1] for flooded conditions. Those shown in Fig. 2a correspond to flow in a direction 54° to the minor axis of the Hertzian ellipse, while those in Fig. 2b relate to flow along the major axis.

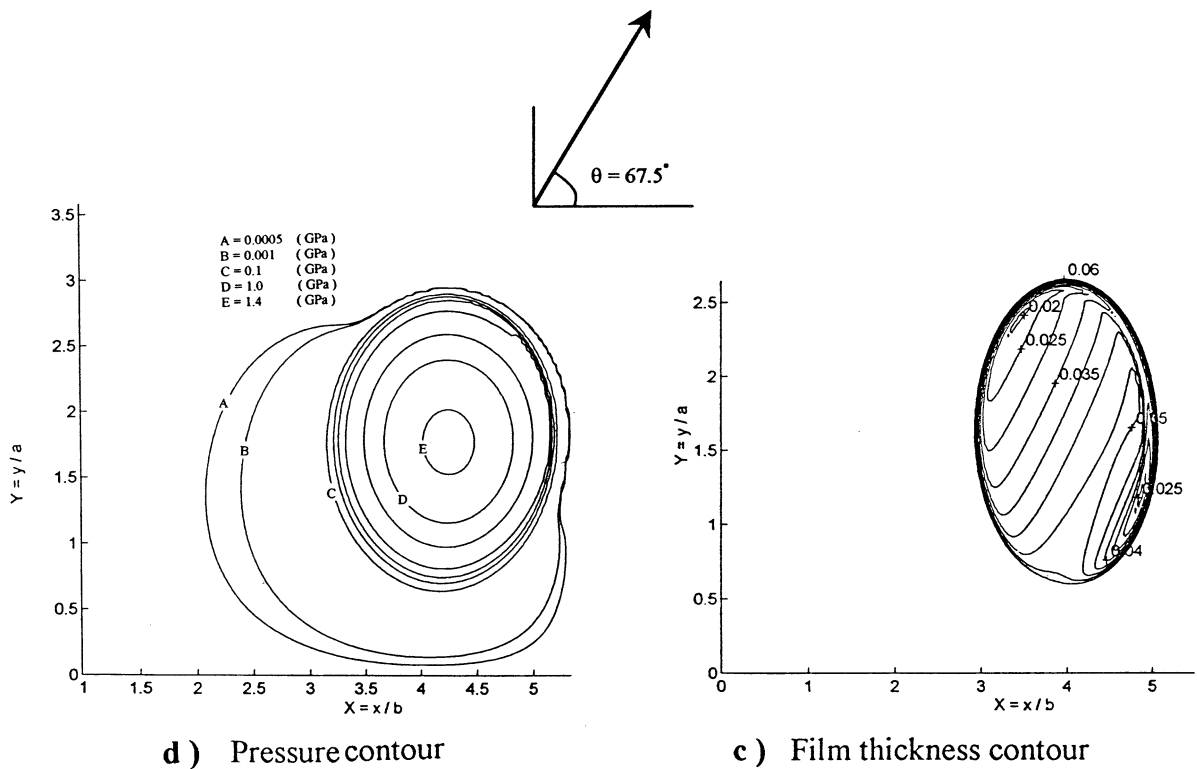
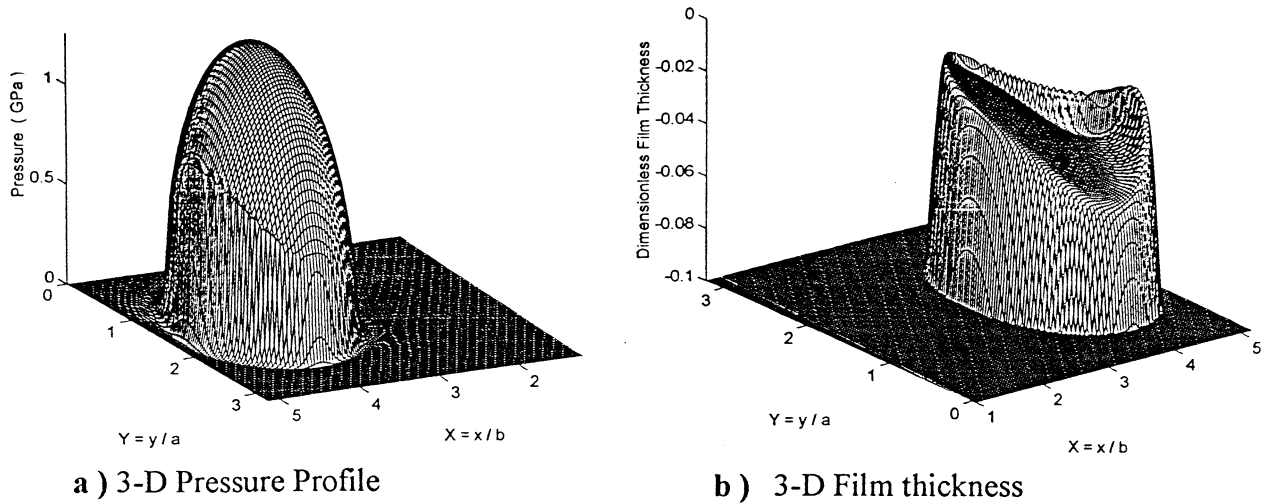


Fig. 1 Pressure profile and film thickness for case (64) in Table 1 ($W = 400$ N, $G^* = 4865$, $\theta = 67.5^\circ$, $U_e = 1$ m/s and $K = 2$)

Good agreement has been observed between the numerical predictions and the experimental results.

Further comparisons have been made with the numerical results reported by Chittenden *et al.* [3, 4]. The comparisons are based upon numerical prediction of the minimum and central oil-film thickness with the extrapolated oil-film formulae in references [2] to [4]. It should be noted that the

formulae in references [2] to [4] are only applicable for low loads. Therefore, it is expected that, with increasing applied load, the aforementioned formulae will consistently overestimate the oil-film thickness. This trend is in fact observed in Figs 3a, b, c, d and e, for flow entrainment along the minor axis, at 22.5° , at 45° , at 67.5° and along the major axis respectively. The largest errors occur at higher

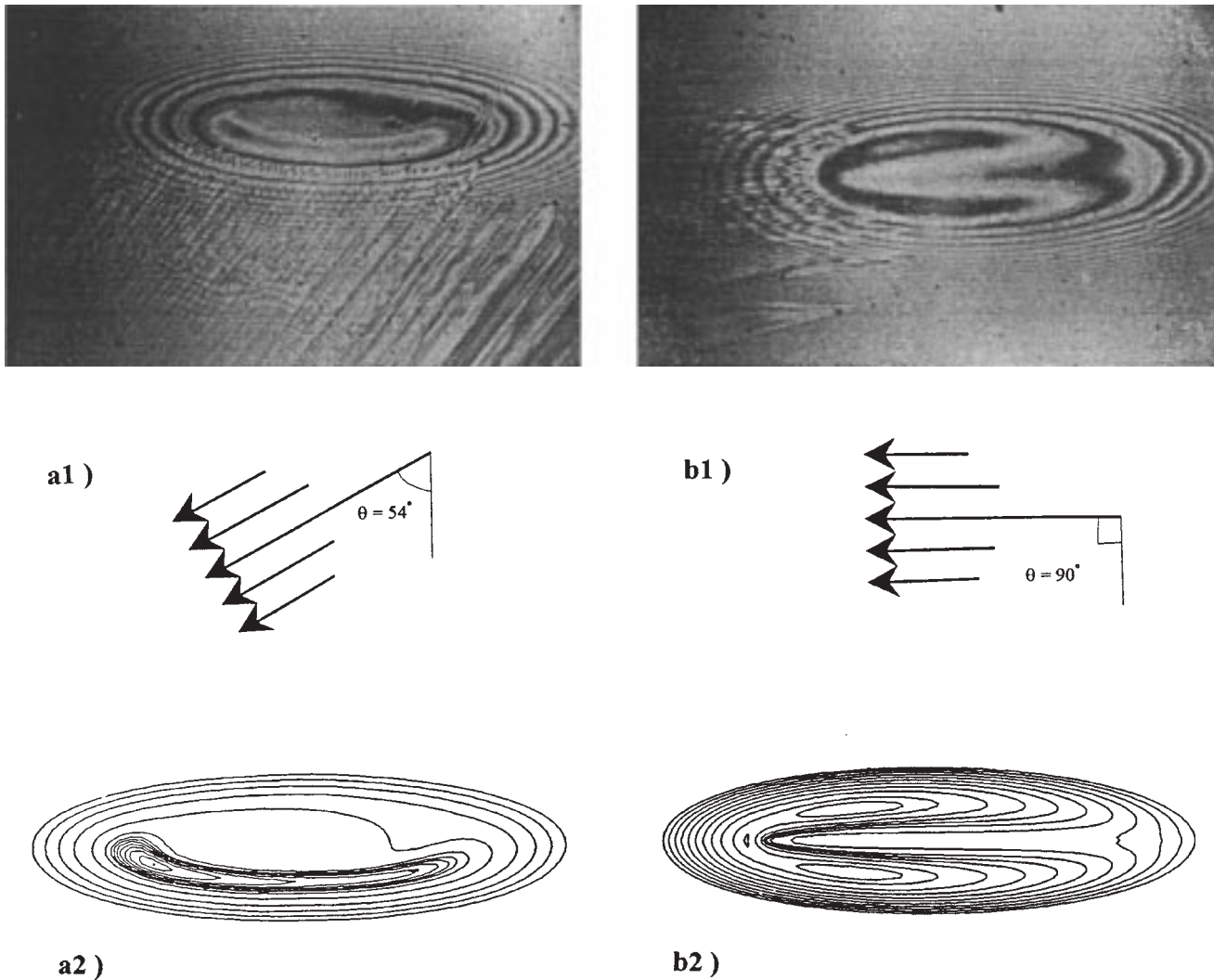


Fig. 2 (a1), (b1) Photographs of experimental contours and (a2), (b2) theoretical oil-film contours: (a) $\theta = 54^\circ$, $G^* = 3865$, $U^* = 2.07 \times 10^{-11}$, $W^* = 0.471 \times 10^{-6}$ and $K = 3.65$; (b) $\theta = 90^\circ$, $G^* = 3412$, $U^* = 3.77 \times 10^{-11}$, $W^* = 7.540 \times 10^{-7}$ and $K = 3.56$

loads and when the flow is along the major axis of the Hertzian ellipse. The maximum error is around 20 per cent. For such thin films, accurate prediction of film thickness is quite important in machinery applications.

A large number of simulation runs under different conditions were undertaken, the results of which are listed in Table 1. Unlike the traditional numerical methods used in references [2] to [4], the numerical method reported in this paper is suitable for the prediction of pressure distribution and film thickness at high loads and low speeds of entraining motion. To illustrate this, a simulation run has been undertaken at a load of 3000 N for a ball of 11 mm radius in a raceway groove, with an ellipticity ratio of 2. The direction of entraining motion is at 45° to the minor axis of the elastostatic contact ellipse. The speed of entraining motion for this condition was set at 2 m/s. Figure 4 shows the contour of the oil film and the

corresponding pressure isobars. It can be observed that the minimum oil-film thickness of $0.2 \mu\text{m}$ has formed in the rear end and to the side of the contact. The pressure distribution is dominated by the primary Hertzian pressure at the centre of the contact with a value of 4 GPa, this being the limiting value of pressure that such a ball would take with subsurface maximum shear stress still remaining within the elastic limit. There is a small pressure spike at the rear exit. The dominance of the primary pressure peak is a feature of highly loaded contacts.

4 CONCLUSION

This paper provides solutions for combined rolling and sliding elliptical point contact conditions, which are

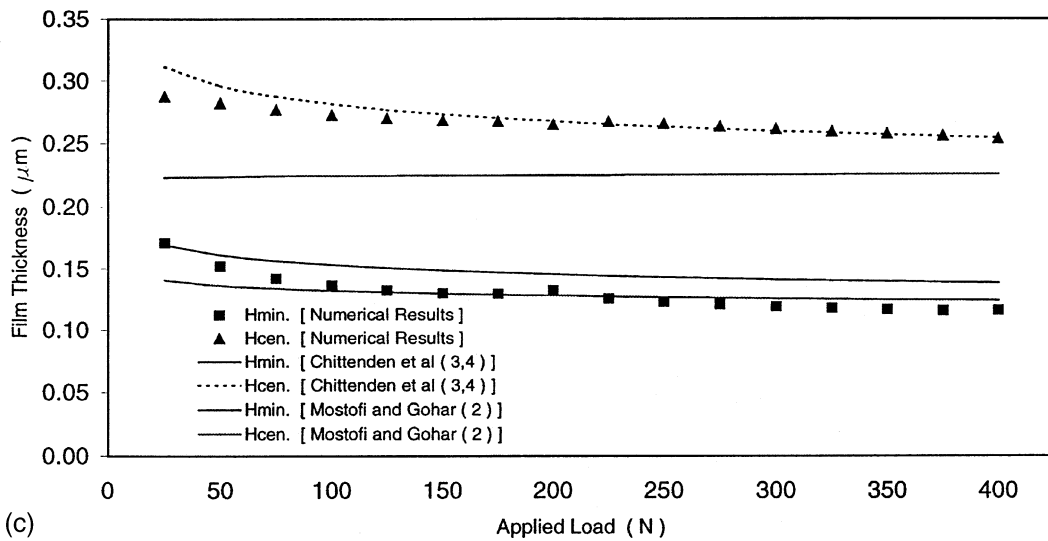
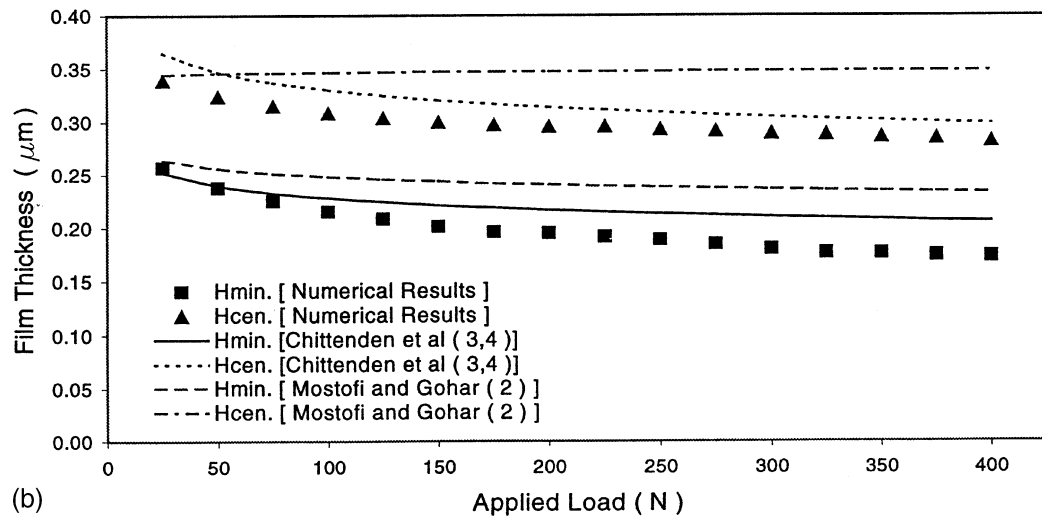
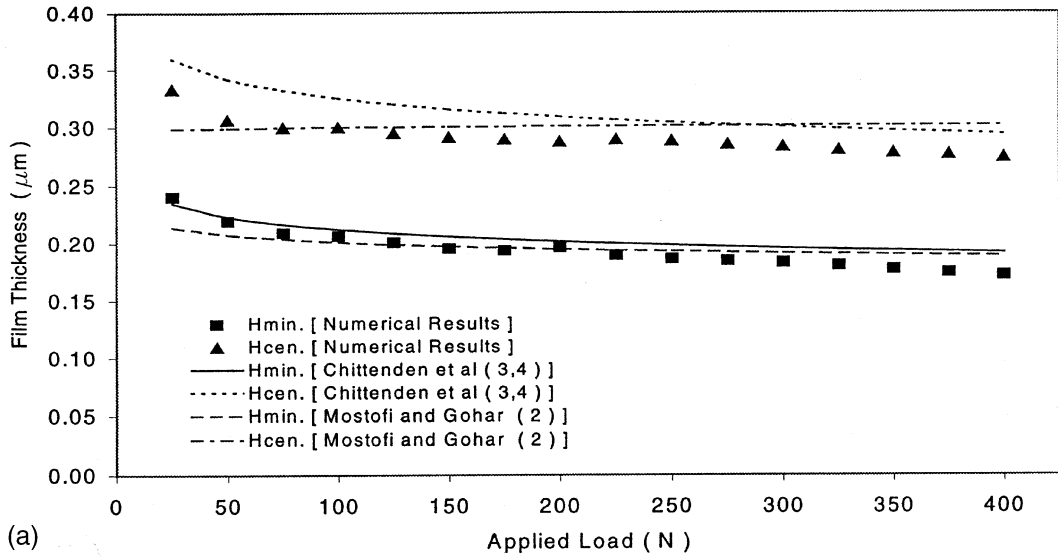
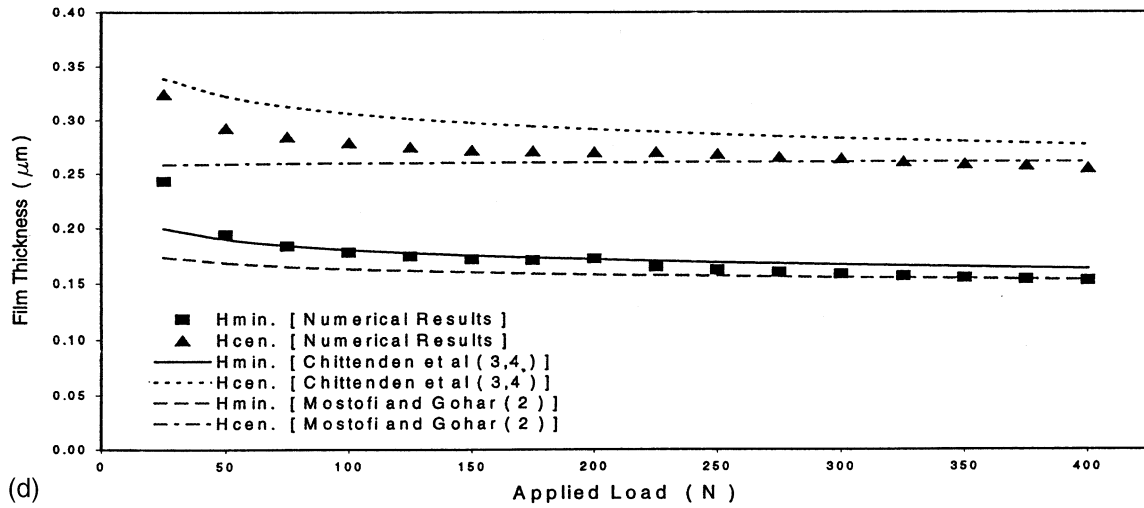
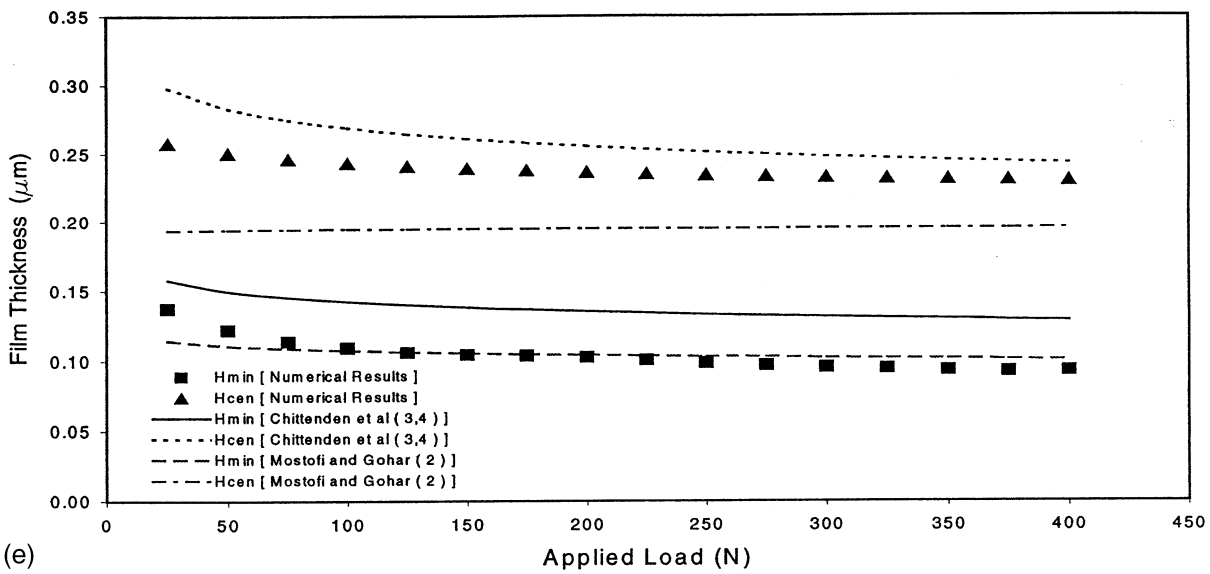


Fig. 3 (continued over)



(d)



(e)

Fig. 3 Variation in the minimum and central film thicknesses with load: (a) $\theta = 0^\circ$, (b) $\theta = 22.5^\circ$, (c) $\theta = 45^\circ$, (d) $\theta = 67.5^\circ$, (e) $\theta = 90^\circ$

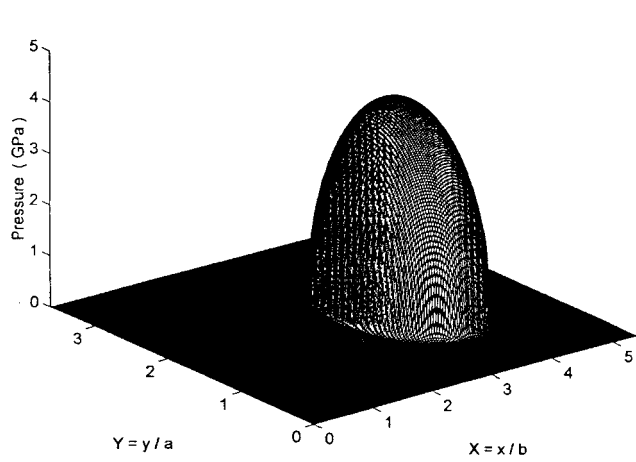
Table 1 Effect of load and entraining direction on the minimum and central film thickness

Set	Entrainment angle (deg)	Case	Parameters					Numerical solution		From references [3] and [4]		From reference [2]	
			K	G^*	W (N)	U_c (m/s)	P_{Hmax} (GPa)	\bar{h}_{min} (μm)	\bar{h}_{cen} (μm)	\bar{h}_{min} (μm)	\bar{h}_{cen} (μm)	\bar{h}_{min} (μm)	\bar{h}_{cen} (μm)
1	0	1	2	4865	25	1.00	0.566	0.257	0.339	0.252	0.365	0.264	0.345
		2			50		0.714	0.238	0.324	0.240	0.347	0.256	0.346
		3			75		0.817	0.225	0.315	0.233	0.337	0.251	0.346
		4			100		0.899	0.215	0.308	0.228	0.330	0.248	0.347
		5			125		0.968	0.208	0.303	0.224	0.325	0.245	0.347
		6			150		1.029	0.201	0.299	0.221	0.321	0.243	0.347
		7			175		1.084	0.196	0.297	0.219	0.317	0.242	0.347
		8			200		1.133	0.195	0.299	0.216	0.314	0.240	0.348
		9			225		1.178	0.191	0.297	0.215	0.311	0.239	0.348
		10			250		1.220	0.188	0.296	0.213	0.309	0.238	0.348
		11			275		1.259	0.184	0.293	0.211	0.307	0.237	0.348
		12			300		1.297	0.180	0.289	0.210	0.305	0.236	0.348
		13			325		1.332	0.176	0.288	0.209	0.303	0.235	0.348
		14			350		1.365	0.173	0.286	0.208	0.301	0.234	0.348
		15			375		1.397	0.169	0.284	0.207	0.300	0.234	0.348
		16			400		1.427	0.167	0.281	0.206	0.298	0.233	0.348

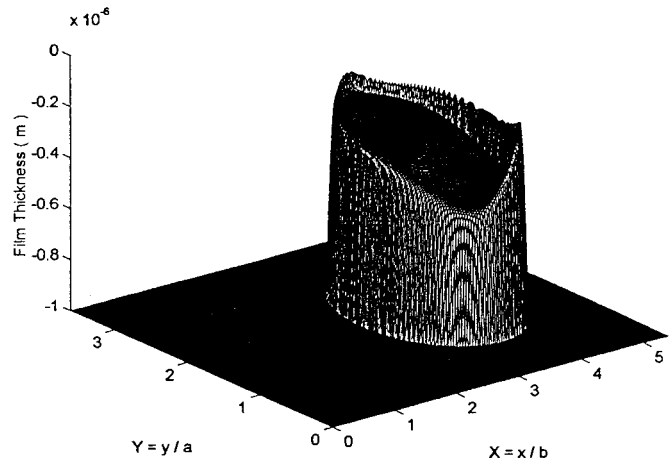
(Continued over)

Table 1 (continued)

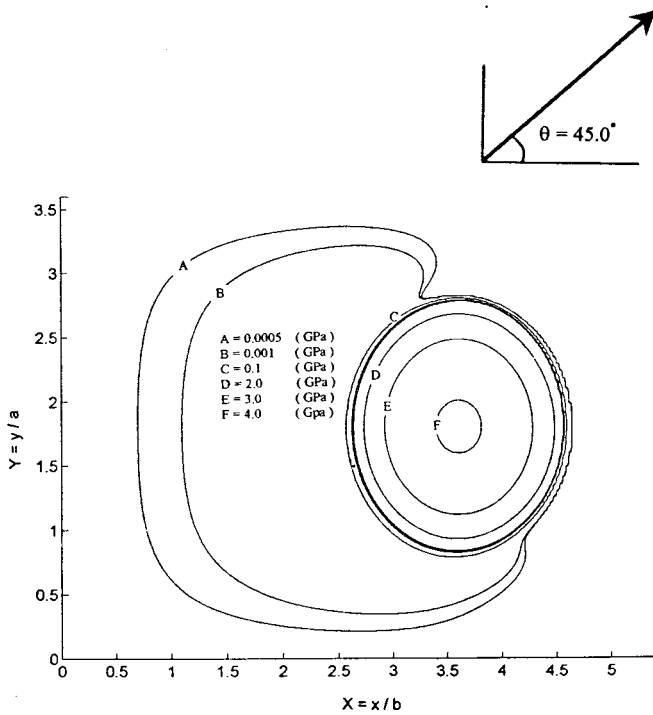
Set	Entrainment angle (deg)	Case	Parameters				Numerical solution		From references [3] and [4]		From reference [2]								
			K	G^*	W (N)	U_e (m/s)	$P_{H \max}$ (GPa)	\bar{h}_{\min} (μm)	\bar{h}_{cen} (μm)	\hat{h}_{\min} (μm)	\hat{h}_{cen} (μm)	\tilde{h}_{\min} (μm)	\tilde{h}_{cen} (μm)						
2	22.5	17	2	4865	25	1.00	0.566	0.240	0.333	0.235	0.360	0.214	0.298						
					50		0.714	0.219	0.306	0.223	0.342	0.207	0.299						
					75		0.817	0.209	0.300	0.216	0.332	0.204	0.300						
					100		0.899	0.207	0.300	0.212	0.325	0.201	0.300						
					125		0.968	0.201	0.295	0.209	0.320	0.199	0.300						
					150		1.029	0.196	0.291	0.206	0.316	0.197	0.300						
					175		1.084	0.194	0.289	0.203	0.312	0.196	0.301						
					200		1.133	0.197	0.288	0.201	0.309	0.195	0.301						
					225		1.178	0.190	0.289	0.200	0.306	0.194	0.301						
					250		1.220	0.187	0.288	0.199	0.304	0.193	0.301						
					275		1.259	0.185	0.285	0.197	0.302	0.192	0.301						
					300		1.297	0.183	0.283	0.196	0.300	0.191	0.301						
					325		1.332	0.181	0.280	0.195	0.298	0.191	0.301						
					350		1.365	0.177	0.278	0.194	0.297	0.190	0.301						
375	1.397	0.175	0.277	0.193	0.295	0.189	0.302												
400	1.427	0.172	0.274	0.192	0.294	0.189	0.302												
3	45	33	2	4865	25	1.00	0.566	0.240	0.333	0.235	0.360	0.174	0.258						
					50		0.714	0.291	0.306	0.223	0.342	0.168	0.259						
					75		0.817	0.209	0.300	0.217	0.332	0.165	0.260						
					100		0.899	0.207	0.300	0.212	0.325	0.163	0.260						
					125		0.968	0.201	0.295	0.209	0.320	0.161	0.260						
					150		1.029	0.196	0.291	0.206	0.316	0.160	0.260						
					175		1.084	0.194	0.289	0.204	0.312	0.159	0.260						
					200		1.133	0.197	0.288	0.202	0.309	0.158	0.260						
					225		1.178	0.190	0.289	0.200	0.306	0.157	0.261						
					250		1.220	0.187	0.288	0.199	0.304	0.157	0.261						
					275		1.259	0.185	0.285	0.197	0.302	0.156	0.261						
					300		1.297	0.183	0.283	0.196	0.300	0.155	0.261						
					325		1.332	0.181	0.280	0.195	0.298	0.155	0.261						
					350		1.365	0.177	0.278	0.194	0.297	0.154	0.261						
					375		1.397	0.175	0.277	0.193	0.295	0.154	0.261						
					400		1.427	0.172	0.274	0.192	0.294	0.153	0.261						
					4		67.5	49	2	4865	25	1.00	0.566	0.171	0.287	0.170	0.312	0.141	0.233
											50		0.714	0.152	0.282	0.161	0.296	0.137	0.224
75	0.817	0.142	0.277	0.157		0.288					0.134		0.224						
100	0.899	0.137	0.272	0.153		0.282					0.132		0.225						
125	0.968	0.133	0.270	0.151		0.277					0.131		0.225						
150	1.029	0.130	0.268	0.149		0.273					0.130		0.225						
175	1.084	0.130	0.268	0.147		0.270					0.129		0.225						
200	1.133	0.132	0.265	0.146		0.268					0.128		0.225						
225	1.178	0.126	0.267	0.144		0.265					0.128		0.225						
250	1.220	0.123	0.266	0.143		0.263					0.127		0.225						
275	1.259	0.121	0.263	0.142		0.261					0.126		0.226						
300	1.297	0.119	0.261	0.141		0.260					0.126		0.226						
325	1.332	0.118	0.259	0.141		0.258					0.125		0.226						
350	1.365	1.117	0.258	0.140		0.257					0.125		0.226						
375	1.397	0.116	0.256	0.139		0.256					0.125		0.226						
400	1.427	0.116	0.354	0.139		0.254					0.124		0.226						
5	90	65	2	4845	25	1.00	0.566	0.137	0.258	0.157	0.298	0.141	0.223						
					50		0.714	0.122	0.250	0.150	0.283	0.137	0.224						
					75		0.817	0.114	0.246	0.145	0.275	0.134	0.224						
					100		0.899	0.109	0.243	0.142	0.269	0.132	0.225						
					125		0.968	0.106	0.241	0.140	0.265	0.131	0.225						
					150		1.029	0.104	0.239	0.138	0.261	0.130	0.225						
					175		1.084	0.104	0.238	0.137	0.258	0.129	0.225						
					200		1.133	0.103	0.237	0.135	0.256	0.128	0.225						
					225		1.178	0.101	0.235	0.134	0.254	0.128	0.225						
					250		1.220	0.0985	0.234	0.133	0.252	0.127	0.225						
					275		1.259	0.0968	0.234	0.132	0.250	0.126	0.226						
					300		1.297	0.0955	0.023	0.131	0.248	0.126	0.226						
					325		1.332	0.0945	0.232	0.131	0.247	0.125	0.226						
					350		1.365	0.0934	0.231	0.130	0.245	0.125	0.226						
					375		1.397	0.0927	0.231	0.129	0.244	0.125	0.226						
					400		1.427	0.0928	0.230	0.129	0.243	0.124	0.226						



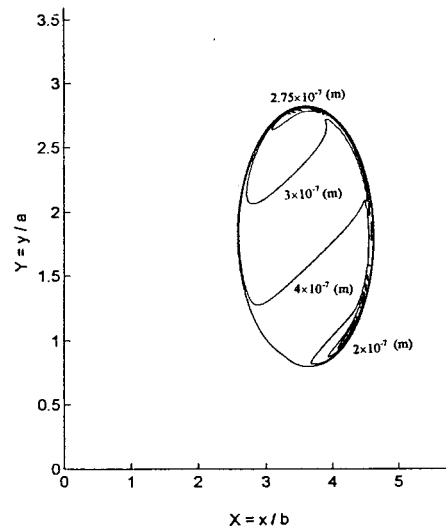
a) 3-D Pressure Profile



b) 3-D Film Thickness



d) Pressure contour



c) Film thickness contour

Fig. 4 Pressure profile and film thickness ($W = 3000$ N, $G^* = 4865$, $\theta = 45^\circ$, $U_c = 2$ m/s, $P_H = 4.0$ GPa and $K = 2$)

prevalent in practice in many lubricated conjunctions. There has been a dearth of research in the study of these conditions, particularly at medium to high loads, which are commonplace in many applications. The available literature in the field report solutions with coarse computational meshes and at low loads, resulting in low contact pressures (typically less than

0.3 GPa in references [2] to [4]). The current solution shows that, under practical conditions, maximum pressures in the region of 4 GPa can be expected. An appropriate numerical method with a fine mesh density has been employed in the current analysis, the results of which show good correlation with the experimental findings.

ACKNOWLEDGEMENTS

The authors would like to express their gratitude to the Iranian Ministry of Culture and Higher Education and the Sahand University of Technology for sponsoring this research project.

REFERENCES

- 1 **Thorp, N.** and **Gohar, R.** Hydrodynamic friction in elliptical and circular point contacts. *Trans. ASME, J. Lubric. Technol.*, July 1971, **94**, 199–208.
- 2 **Mostofi, A.** and **Gohar, R.** Oil film thickness and rolling friction in elastohydrodynamic point contact. *Trans. ASME, J. Lubric. Technol.*, July 1971, **24**, 173–182.
- 3 **Chittenden, R. J., Dowson, D., Dunn, J. F.** and **Taylor, C. M.** A theoretical analysis of the isothermal elastohydrodynamic lubrication of concentrated contacts. Part I: direction of lubricant entrainment coincident with the major axis of the Hertzian contact ellipse. *Proc. R. Soc. Lond. A*, 1985, **397**, 245–269.
- 4 **Chittenden, R. J., Dowson, D., Dunn, J. F.** and **Taylor, C. M.** A theoretical analysis of the isothermal elastohydrodynamic lubrication of concentrated contacts. Part II: general case, with lubricant entrainment along either principal axis of the Hertzian contact ellipse or at some intermediate angle. *Proc. R. Soc. Lond. A*, 1985, **397**, 271–294.
- 5 **Dowson, D.** and **Wang, D.** An analysis of the normal bouncing of a solid elastic ball on an oily plane. *Wear*, 1994, **179**, 29–38.
- 6 **Dowson, D.** and **Higginson, G. R.** A numerical solution to the elastohydrodynamic problem. *J. Mech. Engng Sci.*, 1959, **1**, 6–15.
- 7 **Roelands, C. J. A.** Correlation aspects of viscosity–temperature–pressure relationship of lubricating oils. PhD thesis, Delft University of Technology, The Netherlands, 1966.
- 8 **Jalali-Vahid, D.** Transient analysis of isothermal elastohydrodynamic point contacts. PhD thesis, University of Bradford, 2000.
- 9 **Rahnejat, H.** and **Gohar, R.** The vibrations of radial ball bearings. *Proc. Instn Mech. Engrs, Part C, Journal of Mechanical Engineering Science*, 1985, **199**(C3), 181–193.